Structural dynamics of the myosin relay helix by time-resolved EPR and FRET

Roman V. Agafonov[a], Igor V. Negrashov[a], Yaroslav V. Tkachev[a,b], Sarah E. Blakely[a], Margaret A. Titus[c], David D. Thomas[a,1], and Yuri E. Nesmelov[a,1]

Departments of [a]Biochemistry, Molecular Biology, and Biophysics and [c]Genetics, Cell Biology, and Development, University of Minnesota Medical School, Minneapolis, MN 55455; and [b]Engelhardt Institute of Molecular Biology, Russian Academy of Sciences, Moscow 119991, Russia

Edited by Thomas D. Pollard, Yale University, New Haven, CT, and approved October 5, 2009 (received for review August 26, 2009)

We have used two complementary time-resolved spectroscopic techniques, dipolar electron–electron resonance and fluorescence resonance energy transfer to determine conformational changes in a single structural element of the myosin motor domain, the relay helix, before and after the recovery stroke. Two double-Cys mutants were labeled with optical probes or spin labels, and interprobe distances were determined. Both methods resolved two distinct structural states of myosin, corresponding to straight and bent conformations of the relay helix. The bent state was occupied only upon nucleotide addition, indicating that relay helix, like the entire myosin head, bends in the recovery stroke. However, saturation of myosin with nucleotide, producing a single biochemical state, did not produce a single structural state. Both straight and bent structural states of the relay helix were occupied when either ATP (ADP.BeF$_x$) or ADP.P$_i$ (ADP.AlF$_4$) analogs were bound at the active site. A greater population was found in the bent structural state when the posthydrolysis analog ADP.AlF$_4$ was bound. We conclude that the bending of the relay helix in the recovery stroke does not require ATP hydrolysis but is favored by it. A narrower interprobe distance distribution shows ordering of the relay helix, despite its bending, during the recovery stroke, providing further insight into the dynamics of this energy-transducing structural transition.

dipolar electron–electron resonance | DEER | molecular dynamics simulation | recovery stroke | disorder-to-order transition

Myosin is a molecular motor that generates force on actin in muscle contraction, cell locomotion, and intracellular trafficking. Myosin works cyclically, changing its structure twice per cycle, producing the power stroke and the recovery stroke. These structural changes are modulated by ATP binding and hydrolysis. X-ray crystal structures of myosin in different biochemical states, trapped with nucleotide analogs that are thought to mimic myosin structural intermediates, provide information about the molecular organization and sensitivity to nucleotide binding, but molecular mechanisms of structural transitions in solution remain unknown. Moreover, the relationship between the bound nucleotide and myosin crystal structure is not entirely consistent. For example, two distinct crystal structures were obtained for myosin complexed with ADP.BeF$_x$ nucleotide analog (1, 2). It is not clear whether these differences reflect an intrinsic property of the myosin, or they simply arise from difference in crystallization conditions. As recently reviewed (3), additional insight demands site-directed labeling and spectroscopy, using crystallographic data as a starting point.

Based on myosin crystal structures (4–6) and spectroscopy (7), it has been proposed that the light-chain-binding domain rotates relative to the catalytic domain, causing the myosin head to straighten in the power stroke and bend in the recovery stroke (Fig. 1*A*). These same crystal structures suggest that this transition between straight (M*) and bent (M**) structures reflects a remarkably similar transition in the relay helix (Fig. 1*B*), the 4.7-nm-long α-helix that couples the nucleotide binding site to the light-chain domain through the converter domain (4, 5). The goal of the present study is to test this hypothesis directly in solution during the recovery stroke.

We engineered two double-Cys *Dictyostelium discoideum* myosin mutants, with one labeling site located at the C terminus of the relay helix (K498C) and another within the stable helices on the lower 50K domain (D515C or A639C) (Fig. 1*B*). These cysteines were labeled either with a nitroxide spin label or a donor–acceptor pair. We then measured the interprobe distances with time-resolved EPR [dipolar electron-electron resonance (DEER)] and time-resolved FRET (TR-FRET) to resolve the structural states of the relay helix in different biochemical states of myosin.

Site-directed spectroscopy has been used previously to detect nucleotide-dependent structural transitions within myosin. Fluorescence of single-Trp myosin mutants (9, 10) and EPR of spin labels attached to single-Cys sites (11, 12) have shown nucleotide-dependent changes in the local environment of labeled sites, and previous FRET studies (8, 13) have provided information about the structure of the whole myosin head, but none of these studies resolved the structural states of an individual structural element within myosin. In the present study, we have used time-resolved EPR and TR-FRET to obtain the structural resolution needed to detect motion, disorder, and conformational heterogeneity within a single myosin subdomain, information needed to elucidate the mechanism of interdomain coupling and principles of energy transduction in myosin.

Results

Relay Helix Bending Determined by DEER. DEER is a pulsed EPR spin echo technique that detects distance-dependent dipolar interactions between a pair of electron spins (14). Because of the r^{-3} dependence of the dipolar interaction and the time-resolved detection, this technique reports the distribution of spin–spin distances in the sample with high resolution in the range of 2 to 6 nm (15). Spin-labeled myosin was trapped in distinct biochemical states: M (apo), M.ADP, M.ATP (M.ADP.BeF$_x$), and M.ADP.P$_i$ (M.ADP.AlF$_4$ or M.ADP.V$_i$), and the interprobe distance distributions were measured with DEER (Fig. 2). Data obtained for M.ADP.AlF$_4$ and M.ADP.V$_i$ (trapping a biochemical state analogous to M.ADP.P$_i$) were virtually identical, so only the former analog is reported in this study. For both myosin mutants, nucleotide binding caused faster decay and oscillation of the spin echo amplitude, directly indicating a decrease in the interprobe distance. In comparison with the apo myosin state,

Author contributions: R.V.A., D.D.T., and Y.E.N. designed research; R.V.A., Y.V.T., and Y.E.N. performed research; I.V.N., S.E.B., and M.A.T. contributed new reagents/analytic tools; R.V.A. and Y.E.N. analyzed data; and R.V.A., D.D.T., and Y.E.N. wrote the paper.

The authors declare no conflict of interest.

This article is a PNAS Direct Submission.

[1]To whom correspondence may be addressed. E-mail: ddt@umn.edu or yn@ddt.biochem.umn.edu.

This article contains supporting information online at www.pnas.org/cgi/content/full/0909757106/DCSupplemental.

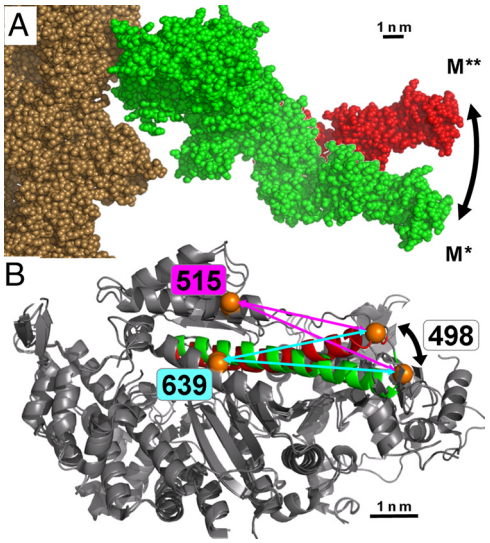

Fig. 1. Proposed coordination of the light-chain domain and the relay helix. (*A*) Myosin S1 bound to actin (brown) in the prerecovery (M*, S1 green) and postrecovery (M**, S1 red) states (3). (*B*) Myosin motor domain, overlay of crystal structures 1FMV (M*, relay helix green) and 1VOM (M**, relay helix red), showing proposed bending of the relay helix. Orange indicates engineered labeling sites, showing predicted shortening of distance between 639 and 498 (cyan arrows) and between 515 and 498 (magenta arrows) during the recovery stroke.

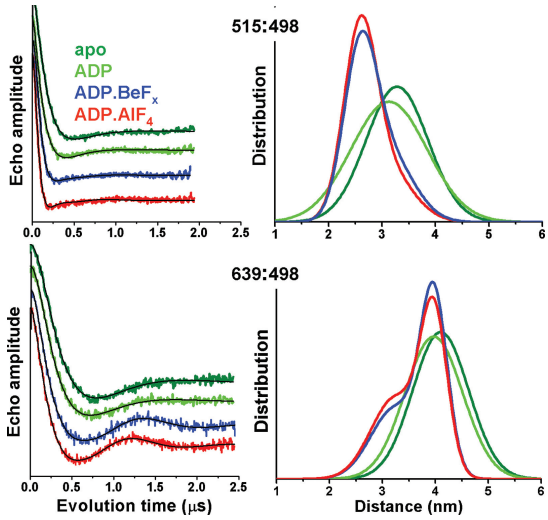

Fig. 2. Bending of the relay helix resolved by DEER. (*Left*) Background-corrected DEER data, obtained from the indicated biochemical states, normalized to constant modulation depth and offset vertically for clarity. (*Right*) Distance distributions extracted from DEER data (M and M.ADP: one-Gaussian distribution, M.ADP.BeF$_X$, M.ADP.AlF$_4$: two-Gaussian distribution). Parameters of distributions are given in Table 1.

ADP had the smallest effect on the DEER data, ADP.AlF$_4$ had the largest effect, and the effect of ADP.BeF$_x$ (analog of ATP) was intermediate (Fig. 2).

Spin echo signals were simulated and fitted to experimental data by assuming Gaussian distributions of distances (Eq. **1**). In the apo state or with bound ADP, a single Gaussian distance distribution was sufficient to produce a good-quality fit. Addition of a second Gaussian distance distribution did not improve the fit (Fig. S1), indicating a single conformation of the relay helix (Fig. 2). The interprobe distance was longest in the apo state, and there was a small, but consistent, decrease of the distance upon ADP binding. When myosin was complexed with ADP.BeF$_x$ or ADP.AlF$_4$, satisfactory fits were obtained only with a two-Gaussian distance distribution, reflecting two structural states of myosin with longer and shorter distances between probes (Fig. S1). All long and short distances extracted from the individual fits of the spin echo signals were similar between M.ADP, M.ADP.AlF$_4$, and M.ADP.Be.F$_x$ complexes. Consequently, signals corresponding to these biochemical states were fitted globally, assuming that the same two states, M* and M** (characterized by the same interprobe mean distances R^* and R^{**}), were present (Fig. 2 and Table 1). The quality of these fits, as judged from the χ^2 values, was comparable with that of unconstrained individual fits, indicating that only two distinct structural states were present (Fig. 3 *A* and *C*).

Relay Helix Becomes More Ordered During the Recovery Stroke. Nucleotide analogs of ATP and ADP.P$_i$ clearly induce not only faster decay rates, but also more pronounced oscillations of the spin echo decay (especially for 639:498, Fig. 2 *Lower*, indicating narrower interprobe distance distributions, compared with apo or ADP-bound states (Fig. 2 *Right*). As illustrated in Fig. 3, it was not possible to fit the data satisfactorily assuming that the widths of the distributions did not change during the myosin structural transition (compare Fig. 3 *A* and *B*). If the width of the M* distribution was allowed to vary, the quality of global fits was equivalent to the quality of unrestricted fits (compare Fig. 3 *A* and *C*). We found that structural flexibility (characterized by the width of the distance distribution) in the M* state was less in the M.ADP.BeF$_x$ and ADP.AlF$_4$ complexes compared with the M.ADP complex. The width of the distance distribution was even narrower in the M** structural state (Fig. 2 *Right* and Table 1).

Relay Helix Bending Determined by TR-FRET. FRET detects the distance r between donor and acceptor probes, coupled by

Table 1. Distance distributions, R (FWHM), and mole fractions observed in each biochemical state, detected by DEER (Fig. 2)

		apo		ADP		ADP.BeF$_x$		ADP.AlF$_4$	
Construct	Structural state	Distance distribution R (FWHM), nm	Fraction	Distance distribution R (FWHM), nm	Fraction	Distance distribution R (FWHM), nm	Fraction	Distance distribution R (FWHM), nm	Fraction
515:498	M	3.28 (1.36)	1.0	-	-	-	-	-	-
	M*	-	-	3.13 (1.53)	1.0	3.13 (1.10)	0.38	3.13 (1.10)	0.28
	M**	-	-	-	-	2.59 (0.73)	0.62	2.59 (0.73)	0.72
639:498	M	4.10 (1.24)	1.0	-	-	-	-	-	-
	M*	-	-	3.97 (1.28)	1.0	3.97 (1.08)	0.58	3.97 (1.08)	0.52
	M**	-	-	-	-	3.24 (0.59)	0.42	3.24 (0.59)	0.48

R, mean distance; FWHM, full width of the Gaussian distribution at half maximum (Eq. **1**); Fraction, mole fraction of myosin (X, X*, X**) occupying a given structural state (M, M*, M**). Experimental conditions are as described in *Materials and Methods*.

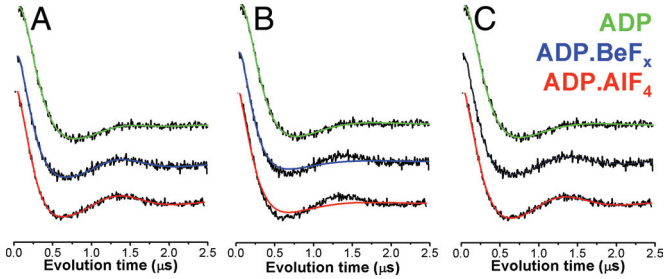

Fig. 3. Fitting of DEER signals in different biochemical states of myosin (639:498 mutant). (*A*) Each signal was fitted independently. (*B*) All signals were fitted globally using one set of parameters: R*, R**, FWHM*, FWHM**. (*C*) All signals were fitted globally using one set of parameters, except that FWHM* for M.ADP was allowed to be different from that for M.ADP.BeF_x and M.ADP.AlF_4. We conclude that the two structural states M* and M** have the same mean distances R* and R** in all three biochemical states, but the width FWHM* of the M* distribution is less in the nucleotide analog biochemical states. The parameters derived from these best fits are summarized in Table 1.

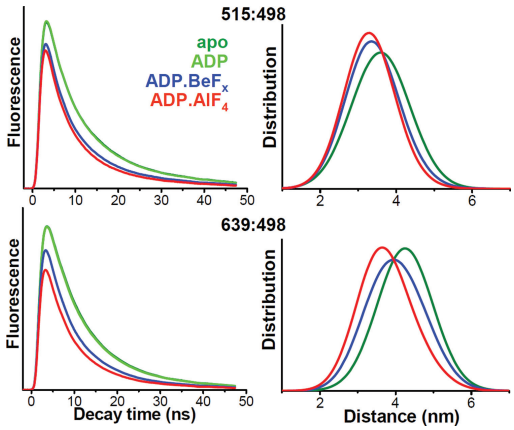

Fig. 4. Bending of the relay helix resolved by TR-FRET. (*Left*) Fluorescence signals of donor–acceptor-labeled myosin mutants in the biochemical states indicated. (*Right*) Distance distributions obtained by fitting fluorescence signals. Parameters of distributions are given in Table 2.

nonradiative energy transfer. As a result of this energy transfer, the rate of the donor's fluorescence decay is increased in proportion to r^{-6}. In the TR-FRET experiment, the donor is excited with a nanosecond laser pulse, its fluorescence is detected with subnanosecond resolution, and the fluorescence lifetime τ is used to calculate the distance r. The major advantage of TR-FRET, compared with conventional FRET (where only steady-state fluorescence intensity is measured), is the ability to resolve multiple protein conformations with distinct interprobe distances, which result in distinct lifetimes (16). Fluorescence signals of donor only [5-({2-[(iodoacetyl)amino]-ethyl}amino)naphthalene-1-sulfonic acid (IAEDANS)] (Fig. S2) and donor–acceptor [IAEDANS–4-((4-(dimethylamino)-phenyl)azo)benzoic acid (DABCYL)]-labeled myosin mutants were acquired in different biochemical states: apo, M.ADP, M.ADP.BeF_x (M.ATP), and M.ADP.AlF_4 (M.ADP.P) (Fig. 4 *Left*). Unlike DEER, TR-FRET was insensitive to ADP binding (Fig. 4), probably because of FRET's inferior distance resolution and the larger size and greater flexibility of attached optical probes. However, binding of ADP.BeF_x and ADP.AlF_4 to myosin substantially decreased the donor lifetime, indicating an increase in FRET efficiency and shortening of the mean distance between probes (Fig. 4), as observed by DEER (Fig. 2). Donor fluorescence signals for all four biochemical states were fitted globally (assuming the presence of the same two structural states: M* and M**) according to Eqs. **2–6** (Fig. 4). Based on comparison of residuals and χ^2 values for one- and two-Gaussian fits (Fig. S3) we concluded that a single structural state is populated in the apo and M.ADP biochemical states, and two structural states are populated with bound ADP.BeF_x and ADP.AlF_4. The mole fractions of myosin populations, interprobe distances, and distance distributions extracted from the fits are shown in Fig. 4 and Table 2.

Discussion

The goal of this study was to determine the structure of the relay helix during the dynamic myosin–nucleotide interaction in solution. The relay helix, an essential element of the force-generating region of myosin, connects the nucleotide binding site and the converter domain. Crystal structures of myosin show two distinct conformations of the relay helix, dependent on the bound nucleotide analog. It is widely assumed that the transition between these myosin conformations, initiated by the myosin–ATP interaction, is the recovery stroke. In this study we ask the following questions: How many structural states are adopted by the relay helix in solution? Is there direct correlation between the state of the nucleotide-binding pocket and the state of the relay helix? How rigid is the relay helix? What initiates the myosin recovery stroke, ATP binding or ATP hydrolysis? We used two complementary spectroscopic probe methods, DEER and FRET, both of which use pulsed excitation and time-resolved detection to obtain structural resolution. For both techniques, two pairs of labeling sites were used to triangulate probe positions in different biochemical states of myosin and unambiguously resolve myosin structural states.

Relay Helix Adopts Two Structural States in Myosin–Nucleotide Complexes. Both DEER and TR-FRET data were in remarkable agreement (Table 3). Both techniques show the presence of two

Table 2. Distance distributions, R (FWHM), and mole fractions observed in each biochemical state, detected by TR-FRET (Fig. 4)

		apo		ADP		ADP.BeF_x		ADP.AlF_4	
Construct	Structural state	Distance distribution R (FWHM), nm	Fraction	Distance distribution R (FWHM), nm	Fraction	Distance distribution R (FWHM), nm	Fraction	Distance distribution R (FWHM), nm	Fraction
515:498	M	3.59 (1.82)	1.0	-	-	-	-	-	-
	M*	-	-	3.59 (1.82)	1.0	3.59 (1.82)	0.45	3.59 (1.82)	0.21
	M**	-	-	-	-	3.24 (1.51)	0.55	3.24 (1.51)	0.79
639:498	M	4.25 (1.73)	1.0	-	-	-	-	-	-
	M*	-	-	4.25 (1.73)	1.0	4.25 (1.73)	0.67	4.25 (1.73)	0.34
	M**	-	-	-	-	3.51 (1.46)	0.33	3.51 (1.46)	0.66

R, mean distance; FWHM, full width of the Gaussian distribution at half maximum (Eq. **1**); Fraction, mole fraction (X, X*, X**) of myosin occupying a given structural state (M, M*, M**). Experimental conditions are as described in *Materials and Methods*.

Table 3. Interprobe distances (nm) in prerecovery (M*) and postrecovery stroke (M) states of myosin determined by different techniques**

Construct	Technique	M*	M**	M*- M**
515:498	X-ray†	3.85	3.12	0.73
	DEER	3.13	2.59	0.54
	FRET	3.59	3.24	0.35
639:498	X-ray†	3.89	3.27	0.62
	DEER	3.97	3.24	0.73
	FRET	4.25	3.51	0.74

†β-carbon distances from 1MMD & 1VOM structures.

structural states of myosin (M* and M**) in a single biochemical (myosin–nucleotide analog) state. These structural states were populated differently, depending on the nucleotide analog bound (ADP.AlF_4, ADP.BeF_x). Apo myosin exhibited one distinct structural state, M. The myosin-ADP biochemical state exhibited a single structural state, M*. The interprobe distance in the M* state was only ≈0.15 nm shorter than in the M state, indicating a subtle change in the relay helix structure after binding of ADP. Only DEER resolves clearly the structural change between M and M* states, probably because of its superior distance resolution and the smaller size of the spin label, compared with the FRET probes. The interprobe distance difference between M* and M** structural states is much more pronounced (≈0.5 nm), reflecting a substantial conformational change of the relay helix. We conclude that there are only two distinct structural states of the force-generating region of myosin in M.ATP and M.ADP.Pi biochemical states, M* and M**. This observation resolves the controversy raised by the observation of two different crystal structures for the same myosin complexed with the same nucleotide analog (ADP.BeF_x) (1, 2). Our results show that both structural states are occupied in solution, so the structure trapped by crystallization probably depends on the specific experimental conditions used for protein preparation and crystal growth.

The Force-Generating Region of Myosin Is More Ordered in the Postrecovery Structural State. Analysis of the interprobe distance distribution in M* and M** structural states shows a narrower width in the postrecovery stroke state M**, indicating more order in the force-generating region of myosin. In agreement with these experimental results, the simulations of myosin molecular dynamics (MD) showed decreased backbone fluctuations in the relay helix in the transition from M* to M** (Fig. 5). In contrast, MD showed no significant effect of this transition on backbone fluctuations at other sites in the lower 50K domain, including the D515 and A639 labeling sites. The N-terminal part of the relay helix is a continuation of the switch II loop, an essential structural element of the nucleotide-binding site of myosin; switch II is open in M* and closed in M**. The experimentally observed narrower distance distribution in the M** structural state (Fig. 2 and Table 1), confirmed by decreased backbone rms fluctuation in MD simulations, reflects the closure of switch II and stronger nucleotide binding.

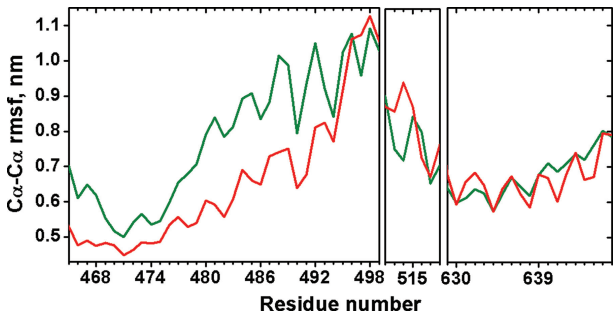

Fig. 5. Simulated backbone fluctuations in prerecovery stroke (green) and postrecovery stroke (red) structural states. Significant differences are seen only in the relay helix (residues 465–499).

ATP Binding Initiates the Recovery Stroke. Our results show that the relay helix responds to changes in the state of the nucleotide binding pocket and identify the relay helix as an interdomain linker that propagates changes from the active site to the converter domain of myosin. Strikingly, we found that with an ATP analog (ADP.BeF_x) bound at the active site, the myosin relay helix can adopt both prerecovery and postrecovery structural states. In contrast to the classic model of myosin function, in which ATP hydrolysis is coupled to a recovery stroke and serves as its driving force, our observations show that ATP binding plays the crucial role in the recovery stroke. The recovery stroke precedes hydrolysis and occurs with ATP bound in the active site. Consequently, hydrolysis is needed not to fuel the recovery stroke but to facilitate product release and continue the cycle. This hypothesis was previously proposed based on MD simulations (17, 18) and crystal structures, which suggested that switch II in the nucleotide pocket must be closed for myosin to be in the catalytically active form (5, 19). Relaxation experiments with single Trp mutants and nucleotide analogs (20) showed changes in intrinsic myosin fluorescence after rapid jump in temperature or pressure. This was attributed to the presence of an equilibrium between the open (prerecovery) and closed (postrecovery) conformations and was used to calculate the equilibrium constants between states. Our distance measurements provide the necessary dimensional details to resolve the two coexisting structural states and determine directly the position of the relay helix in each of the states.

DEER and TR-FRET Are Complementary. Although the two methods both use pulsed excitation and time-resolved detection and the same labeling sites, each has distinct advantages. Compared with relatively simple exponential decays of donor fluorescence in FRET experiments, the complex shape of modulated echo intensity signals in DEER has more distinct spectral features that can be used to evaluate the quality of the fit, providing higher structural resolution. Another DEER advantage is in labeling: the smaller probe size and the ability to use the same probe at both locations (compared with donor–acceptor pairs in FRET) simplify sample preparation and result in more reliable data interpretation. In particular, only DEER detected subtle (≈0.1 nm) changes in structure upon binding of ADP, showed a significant decrease in distribution width in the M.ADP.BeF_x and M.ADP.AlF_4 states, and unambiguously resolved two structural states in myosin–nucleotide analog complexes. However, TR-FRET experiments can be performed at physiological temperatures and have several orders of magnitude higher sensitivity, yielding information about the distance distribution in a single 50-ns signal, detected with subnanosecond resolution. Thus, FRET has the potential to provide this structural resolution in real time during a biochemical transient. In addition, the FRET measurements can be used to establish an upper bound for the transition rate between the resolved conformations, which is approximately the inverse of the average observed fluorescence lifetime. For example, the two conformations resolved in Table 2 must be exchanging more slowly than ≈10^8 s^{-1}.

Conclusions

We have designed myosin constructs to measure nucleotide-induced dynamics of the myosin relay helix, an important structural element in the force-generating region, connecting the nucleotide binding site and the lever arm. Combining protein

mutagenesis, site-directed labeling, high-resolution pulsed EPR spectroscopy (DEER), and high-sensitivity fluorescence spectroscopy (TR-FRET) we (*i*) detected structural changes (bending and ordering) in the myosin relay helix in response to nucleotide analog binding, (*ii*) resolved two structural states (straight and bent) of the relay helix in a single biochemical state of myosin with bound nucleotide analog, and (*iii*) detected changes in order and interprobe distances during the myosin–ATP interaction. We conclude that (*i*) the bending (structural state) of the relay helix is only loosely coupled to the identity of the bound nucleotide (biochemical state), and (*ii*) the bent state of the relay helix is partially populated immediately upon ATP binding to myosin, without requiring ATP hydrolysis. The wider distribution of interprobe distances in the prerecovery stroke states indicates flexibility of the N-terminal part of the relay helix, when the switch II loop in the nucleotide binding site is open. These results provide direct information about the structural dynamics of the relay helix in myosin in solution, providing insight into the interaction between myosin's active site and force-generating region.

Materials and Methods

Protein Preparation and Labeling. Mutants of *D. discoideum* myosin were constructed and purified as described (21). For DEER, the protein was labeled with 4-maleimido-2,2,6,6-tetramethyl-1-piperidinyloxy spin label (MSL) by incubating 100 μM myosin with 600 μM MSL for 12 h on ice, resulting in labeling of >90% of Cys, as measured by mass spectrometry and spectral intensity. For FRET, the protein was labeled in two steps. First, 50 μM myosin was incubated with 45 μM donor (IAEDANS) for 12 h. Then this protein was diluted to 25 μM and incubated with 100 μM acceptor (DABCYL). After each labeling step, unreacted label was removed with size-exclusion spin columns (Pierce). The extent of FRET labeling, determined from dye absorbance, was typically ≈30–40% donor and 60–70% acceptor, with virtually all cysteines being labeled. Labeling buffer contained 20 mM Mops, 50 mM KCl, 3 mM $MgCl_2$, and 1 mM EDTA, pH 7.5. Complexes of myosin with nucleotide analogs were obtained as described (12). Unless indicated otherwise, all experiments were performed at 20 °C in a buffer containing 20 mM *N*-(2-Hydroxyethyl)-piperazine-*N*′-3-propanesulfonic acid (EPPS), 6 mM $MgCl_2$, and 1 mM EGTA, pH 8.0.

ATPase Assays. Myosin ATPase activity was measured in physiological buffer (T = 25 °C in 10 mM Tris, 3 mM $MgCl_2$, and 5 mM ATP, pH 7.5) in the presence and absence of actin, by the liberation of inorganic phosphate (22). The dependence of myosin ATPase activity on actin concentration was fitted by the Michaelis–Menten equation, to determine V_{max} (activity at saturating actin) and K_m (actin concentration at $V = 0.5\ V_{max}$) (details are in Table S1).

Interprobe Distance Distribution. To reflect flexibility in the protein structure, both DEER and FRET signals were simulated by using a set of distance distributions rather than a set of discrete distances. The shape of each distribution was assumed to be Gaussian:

$$\rho(r) = \frac{1}{\sigma\sqrt{2\pi}}\exp\left(-\frac{(r-R)^2}{2\sigma^2}\right), \qquad \sigma = \frac{FWHM}{2\sqrt{2\ \ln 2}}, \qquad [1]$$

where σ is the standard deviation and FWHM is the full width at half maximum.

DEER. Time-resolved DEER signals were acquired with an Elexsys E580 spectrometer (Bruker Biospin) equipped with a dielectric resonator (MD-5; Bruker Biospin), using a four-pulse DEER sequence (23) with a 16-ns π/two pulse, and a 40- to 48-ns ELDOR pulse. The pump frequency was centered on the central resonance of the nitroxide spin label, and the observe frequency was set to the low-field resonance 67 MHz away. Temperature during the acquisition was set to 65° K. Myosin samples (50–75 μM) were flash-frozen in liquid nitrogen before being placed in the spectrometer. Buffer contained 20 mM EPPS, 6 mM $MgCl_2$, 1 mM EGTA, and 10% glycerol (pH 8.0). Spin echo signals were analyzed with the DeerAnalysis software suite (24), which fits simulated DEER signals to the data, assuming one or two Gaussian interprobe distance distributions (Eq. **1**).

TR-FRET. Fluorescence of AEDANS-myosin was excited with the third harmonics of a passively Q-switched microchip YAG laser (NanoUV-355; JDS Uniphase), operated at a pulse repetition rate of 10 kHz, and selected with a 420-nm long-pass glass filter. To avoid anisotropy effects, fluorescence was passed through a polarizer oriented at the magic angle. Fluorescence signals were detected after every laser shot with a photomultiplier module Hamamatsu H5773-20 (rise time 0.78 ns) and acquired with a transient digitizer (Acqiris DC252) with sampling resolution 0.125 ns. The instrument response function (IRF) was acquired with scattered light at the same instrument settings as in the fluorescence measurement, except that there was no emission filter and the emission polarization was vertical.

Analysis of TR-FRET Data. The observed donor-only fluorescence signal $F_{Dobs}(t)$ from labeled myosin was fitted by a simulation $F_{Dsim}(t)$, consisting of a multiexponential decay $F_D(t)$, convolved with the IRF:

$$F_D(t) = \sum_{i=1}^{n} A_i \exp\left(-\frac{t}{\tau_{Di}}\right), \qquad [2]$$

$$F_{D,sim}(t) = \int_{-\infty}^{+\infty} IRF(t-t')\cdot F_D(t')dt', \qquad [3]$$

where τ_{Di} are the donor-only fluorescence lifetimes. We found that two exponential components ($n = 2$ in Eq. **2**) were sufficient; i.e., addition of a third component to the fit did not reduce the residual or χ^2. For each biochemical state the fluorescence signal of donor—acceptor- labeled myosin before convolution, $F_{DA}(t)$, was analyzed by assuming that the only change in $F_D(t)$ was an increased rate of decay caused by energy transfer $k_T = \int k_{Di}[\rho(r)/R_{0i}]^{-6}dr$, where $\rho(r)$ is the donor–acceptor distance distribution (Eq. **1**), $k_{Di} = 1/\tau_{Di}$, and R_{0i} is the Förster distance defined by (Eq. **S1**, Fig. S4).

$$F_{DA}(t) = \int_{-\infty}^{+\infty} \rho(r)\cdot\sum_{i=1}^{n} A_i \exp\left(-\frac{t}{\tau_{Di}} - \frac{t}{\tau_{Di}}\left(\frac{R_{0i}}{r}\right)^6\right)dr, \qquad [4]$$

The observed donor–acceptor fluorescence signal before convolution, $F_{D+A}(t)$, was assumed to be a sum of three terms:

$$F_{D+A}(t) = X_D\cdot F_D(t) + X^*\cdot F^*_{DA}(t, R^*, FWHM^*) + X^{**}\cdot F^{**}_{DA}(t, R^{**}, FWHM^{**}), \qquad [5]$$

$$F_{D+A,sim}(t) = \int_{-\infty}^{+\infty} IRF(t-t')\cdot F_{D+A}(t')dt', \qquad [6]$$

where X^* and X^{**} ($X^* + X^{**} = 1$) are mole fractions of myosin in the prerecovery (straight relay helix) and postrecovery (bent relay helix) state, and X_D is the mole fraction of donor-only labeled myosin ($X^{D+X}DA = 1$).

Observed fluorescence signals in the presence and absence of acceptor were fitted globally (simultaneously) by the simulated expressions in Eqs. **3** and **6**. Intensities A_i, lifetimes τ_i, distances R^* and R^{**}, widths FWHM* and FWHM**, and the fraction X_D of donor-only labeled myosin were linked and varied simultaneously. X^{**} (the fraction of the M^{**} structural state) was varied independently for every signal in the global fit.

For more details see *SI Text*.

ACKNOWLEDGMENTS. We thank Eunice Song and Octavian Cornea for technical assistance. The time-resolved fluorescence instrument used was inspired by numerous insightful discussions with Gregory D. Gillispie, of Fluorescence Innovations, Inc. This work was supported by National Institutes of Health Grants AR32961 (to D.D.T.) and AR53562 (to Y.E.N.) and a grant from the Minnesota Medical Foundation (to Y.E.N.). MD simulations were performed by using the computational resources of the University of Minnesota Supercomputing Institute.

1. Fisher AJ, et al. (1995) X-ray structures of the myosin motor domain of *Dictyostelium discoideum* complexed with MgADP.BeFx and MgADP.AlF4. *Biochemistry* 34:8960–8972.
2. Holmes KC (1998) Muscle contraction. *Novartis Found Symp* 213:76–89; discussion 89–92.
3. Thomas DD, Kast D, Korman VL (2009). Site-directed spectroscopic probes of actomyosin structural dynamics. *Annu Rev Biophys* 38:347–369.
4. Bauer CB, Holden HM, Thoden JB, Smith R, Rayment I (2000) X-ray structures of the apo and MgATP-bound states of *Dictyostelium discoideum* myosin motor domain. *J Biol Chem* 275:38494–38499.
5. Smith CA, Rayment I (1996) X-ray structure of the magnesium(II).ADP.vanadate complex of the *Dictyostelium discoideum* myosin motor domain to 1.9-Å resolution. *Biochemistry* 35:5404–5417.
6. Rayment I, et al. (1993) Three-dimensional structure of myosin subfragment-1: A molecular motor. *Science* 261:50–58.
7. Baker JE, Brust-Mascher I, Ramachandran S, LaConte LE, Thomas DD (1998) A large and distinct rotation of the myosin light chain domain occurs upon muscle contraction. *Proc Natl Acad Sci USA* 95:2944–2949.
8. Shih WM, Gryczynski Z, Lakowicz JR, Spudich JA (2000) A FRET-based sensor reveals large ATP hydrolysis-induced conformational changes and three distinct states of the molecular motor myosin. *Cell* 102:683–694.
9. Malnasi-Csizmadia A, Woolley RJ, Bagshaw CR (2000) Resolution of conformational states of *Dictyostelium* myosin II motor domain using tryptophan (W501) mutants: Implications for the open-closed transition identified by crystallography. *Biochemistry* 39:16135–16146.
10. Yengo CM, Chrin LR, Rovner AS, Berger CL (2000) Tryptophan 512 is sensitive to conformational changes in the rigid relay loop of smooth muscle myosin during the MgATPase cycle. *J Biol Chem* 275:25481–25487.
11. Ostap EM, White HD, Thomas DD (1993) Transient detection of spin-labeled myosin subfragment 1 conformational states during ATP hydrolysis. *Biochemistry* 32:6712–6720.
12. Agafonov RV, Nesmelov YE, Titus MA, Thomas DD (2008) Muscle and nonmuscle myosins probed by a spin label at equivalent sites in the force-generating domain. *Proc Natl Acad Sci USA* 105:13397–13402.
13. Suzuki Y, Yasunaga T, Ohkura R, Wakabayashi T, Sutoh K (1998) Swing of the lever arm of a myosin motor at the isomerization and phosphate-release steps. *Nature* 396:380–383.
14. Milov AD, Ponomarev AB, Tsvetkov YD (1984) Electron–electron double resonance in electron spin echo: Model biradical systems and the sensitized photolysis of decalin. *Chem Phys Lett* 110:67–72.
15. Klein JC, et al. (2008) Actin-binding cleft closure in myosin II probed by site-directed spin labeling and pulsed EPR. *Proc Natl Acad Sci USA* 105:12867–12872.
16. Lakowicz JR, et al. (1990) Conformational distributions of melittin in water/methanol mixtures from frequency-domain measurements of nonradiative energy transfer. *Biophys Chem* 36:99–115.
17. Fischer S, Windshugel B, Horak D, Holmes KC, Smith JC (2005) Structural mechanism of the recovery stroke in the myosin molecular motor. *Proc Natl Acad Sci USA* 102:6873–6878.
18. Cecchini M, Houdusse A, Karplus M (2008). Allosteric communication in myosin V: From small conformational changes to large directed movements. *PLoS Comput Biol* 4:e1000129.
19. Geeves MA, Holmes KC (1999) Structural mechanism of muscle contraction. *Annu Rev Biochem* 68:687–728.
20. Malnasi-Csizmadia A, et al. (2001) Kinetic resolution of a conformational transition and the ATP hydrolysis step using relaxation methods with a *Dictyostelium* myosin II mutant containing a single tryptophan residue. *Biochemistry* 40:12727–12737.
21. Korman VL, Anderson SE, Prochniewicz E, Titus MA, Thomas DD (2006) Structural dynamics of the actin-myosin interface by site-directed spectroscopy. *J Mol Biol* 356:1107–1117.
22. Lanzetta PA, Alvarez LJ, Reinach PS, Candia OA (1979) An improved assay for nanomole amounts of inorganic phosphate. *Anal Biochem* 100:95–97.
23. Pannier M, Veit S, Godt A, Jeschke G, Spiess HW (2000) Dead-time free measurement of dipole–dipole interactions between electron spins. *J Magn Reson* 142:331–340.
24. Jeschke G, et al. (2006) Deer Analysis 2006—a comprehensive software package for analyzing pulsed ELDOR data. *Appl Magn Reson* 30:473–498.